©ESO 2026

Cosmoglobe DR2. V. Spatial correlations between thermal dust and ionized carbon emission in *Planck* HFI and COBE-DIRBE

E. Gjerløw[1]⋆, R. M. Sullivan[1], R. Aurvik[1], A. Basyrov[1], L. A. Bianchi[1], A. Bonato[2], M. Brilenkov[1], H. K. Eriksen[1], U. Fuskeland[1],
M. Galloway[1], K. A. Glasscock[1], L. T. Hergt[3], D. Herman[1], J. G. S. Lunde[1], M. San[1], A. I. Silva Martins[1], D. Sponseller[4], N.-O. Stutzer[1],
H. Thommesen[1], V. Vikenes[1], D. J. Watts[1], I. K. Wehus[1], and L. Zapelli[2,5,6]

[1] Institute of Theoretical Astrophysics, University of Oslo, Blindern, Oslo, Norway
[2] Dipartimento di Fisica, Università degli Studi di Milano, Via Celoria, 16, Milano, Italy
[3] Laboratoire de Physique des 2 infinis – Irène Joliot Curie (IJCLab), Orsay, France
[4] Department of Space, Earth and Environment, Chalmers University of Technology, Gothenburg, Sweden
[5] Università di Trento, Università degli Studi di Milano, CUP E66E23000110001
[6] INFN sezione di Milano, 20133 Milano, Italy

January 13, 2026

ABSTRACT

We fit five tracers of thermal dust emission to ten *Planck* HFI and *COBE*-DIRBE frequency maps between 353 GHz and 25 THz, aiming to map the relative importance of each physical host environment as a function of frequency and position on the sky. Four of these correspond to classic thermal dust tracers, namely H ɪ (HI4PI), CO (Dame et al. 2001a), Hα (WHAM, Haffner et al. (2003a, 2016)), and dust extinction (*Gaia*; Edenhofer et al. 2024), while the fifth is ionized carbon (C ɪɪ) emission as observed by *COBE*-FIRAS. To our knowledge, this has until now been considered to be primarily a gas tracer, rather than a dust tracer. After smoothing all data to the common resolution of the FIRAS experiment, and subtracting subdominant astrophysical components as appropriate for each channel (cosmic microwave and infrared backgrounds, and zodiacal light), we jointly fit these five templates to each frequency channel through standard multi-variate linear regression. At frequencies higher than 1 THz, we find that the dominant tracer is in fact C ɪɪ, and above 10 THz this component accounts for almost the entire fitted signal; at frequencies below 1 THz, its importance is second only to H ɪ. We further find that all five components are well described by a modified blackbody spectral energy density (SED) up to some component-dependent maximum frequency ranging between 1 and 5 THz. In this interpretation, the C ɪɪ-correlated component is the hottest among all five, with an effective temperature of about 25 K. For comparison, the H ɪ and CO components have effective temperatures of 16 K and 12 K, respectively. The Hα component has a temperature of 18 K, and, unlike the other four, is observed in absorption rather than emission. The spectral indices of the five components range between $\beta = 1.4$ (for H ɪ) and 2.6 (for Hα); for the C ɪɪ component, $\beta = 1.56$. Despite the simplicity of this model, which relies only on external templates coupled to spatially isotropic SEDs, we find that it captures 98 % of the full signal root mean squared (RMS) below 1 THz. At higher frequencies, which are more susceptible to non-thermal emission processes, the model still captures more than 80 % of the full signal RMS. This high efficiency suggests that spatial variations in the thermal dust SED, as for instance reported by *Planck* and other experiments, may be more economically modelled on large angular scales in terms of a spatial mixing of individually isotropic physical components, than by a single uniform well-mixed interstellar medium coupled to a spatially varying temperature field, as has been the norm until now. Indeed, the results found in this paper motivate the thermal dust model adopted for the Cosmoglobe DR2 re-analysis of the *COBE*-DIRBE data, and we believe that they may also provide inspiration for refining both current theoretical interstellar medium models and component separation algorithms in general.

Key words. ISM: general - Zodiacal dust, Interplanetary medium - Cosmology: observations, diffuse radiation - Galaxy: general

1. Introduction

The interstellar medium (ISM) plays a ubiquitous role in modern astrophysics and cosmology across the electromagnetic spectrum (e.g., Draine 2011, Hensley & Draine 2023). On one hand, understanding the composition and physics of the ISM informs us about the structure and dynamics of both the Milky Way and distant galaxies, and ISM studies are therefore an important and interesting field of astronomy in their own right. On the other hand, ISM radiation is a key contaminant for a broad range of other high-impact science targets, for instance the search for gravitational waves in the cosmic microwave background (CMB), dark matter annihilation in gamma-ray observations, or

dark energy constraints through high-precision measurements of distant supernovae. Accurate ISM modelling is therefore a key aspect in 21st century astrophysics.

Broadly speaking, the ISM is comprised of cosmic rays (relativistic particles), gas (atoms or small molecules), and dust (large molecules, typically ranging in size from a few angstroms to $100 \, \mu m$). All of these emit electromagnetic radiation at various frequencies, for instance through synchrotron, bremsstrahlung, quantum mechanical line emission, or thermal emission. In addition, dust grains absorb electromagnetic radiation with wavelengths that are comparable to the grain size, which due to the grain distribution happens most notably in wavelengths ranging from infrared to X-rays.

The current paper is part of a suite of seven companion papers that describes the Cosmoglobe Data Release 2 (DR2; Watts
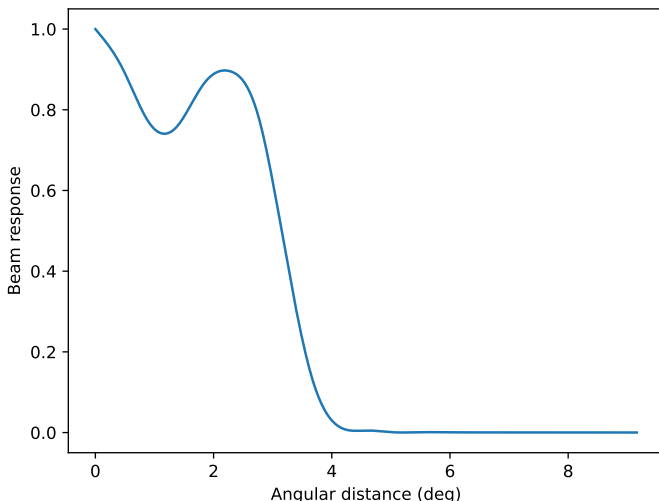

Fig. 1. The *COBE*-FIRAS beam, with which all maps in this analysis were smoothed. The beam diameter is around 7° on the sky, which limits this analysis to N_{side}=16.

et al. 2024a). The primary main goal of this work is to reanalyze the *COBE*-DIRBE data (Hauser et al. 1998) within a global Bayesian end-to-end analysis framework, and use the resulting data to constrain the spectrum of the cosmic infrared background (CIB; Watts et al. 2024b). The DIRBE instrument observed the full sky in 10 wavelength bands covering 1.25 and 240 μm. By virtue of covering virtually the entire infrared regime, DIRBE is an excellent dust tracer, both originating from the Milky Way and from within the Solar system. Indeed, while DIRBE's original science goal was to detect and characterize the CIB spectrum and fluctuations, the longest lasting legacy of the survey has arguably been to serve as a unique well-calibrated full-sky tracer of dust emission in the Milky Way (Schlegel et al. 1998; Miville-Deschênes & Lagache 2005; Planck Collaboration X 2016; Sano et al. 2016; Pan-Experiment Galactic Science Group 2025) and zodiacal light emission (e.g., Kelsall et al. 1998; Planck Collaboration XIV 2014; Kondo et al. 2016; San et al. 2024; O'Brien et al. 2025).

One of the many important questions in which the DIRBE data has played a role regards the nature and composition of thermal dust emission in the far-infrared regime, and how it may be modelled most efficiently. Early studies quickly suggested that a single so-called modified blackbody (MBB) spectrum provided a good fit to the thermal dust spectral energy density (SED) for a broad range of frequencies (Reach et al. 1995). An MBB spectrum has three degrees of freedom, namely an overall amplitude (tracing the density of the medium), an effective temperature, and a spectral index. To this date, the single-component MBB model plays a key role in both microwave modelling and infrared-based dust studies.

However, it also quickly became clear that the validity of a single MBB spectrum is limited in frequencies. Notably, in a seminal paper Finkbeiner et al. (1999) presented a two-component MBB thermal dust model derived from the *IRAS* 100 μm and DIRBE 100 and 240 μm data that served as a benchmark for the CMB community for more than a decade, and was only superseded by the far more sensitive *Planck* HFI data (Planck Collaboration XI 2014). Since that time, the combination of *Planck*, DIRBE, and *IRAS* measurements have dominated the study of large-scale dust emission at microwave and far-infrared frequencies.

Despite massive efforts developing increasingly more accurate and well-defined models of thermal dust emission, combining theoretical insights with observational constraints (e.g., Draine 2011; Hensley & Draine 2023), many critical questions plague this field to date. Furthermore, the importance of understanding microwave dust emission has only increased in recent years, as the attention of the CMB field has shifted to the search for inflationary gravitational waves through *B*-mode polarization constraints (e.g., BICEP2 Collaboration 2018; Ade et al. 2019; LiteBIRD Collaboration et al. 2023). For such experiments, polarized thermal dust emission represents one of the most important contaminants, and major resources are currently being invested in devising both instrumentation and data analysis techniques to handle this challenge.

In the current paper, and in two companion papers by Sullivan et al. (2026) and Gjerløw et al. (2026), we revisit the question of how to model thermal dust emission efficiently in light of the currently reprocessed DIRBE data, jointly with archival measurements from *Planck* HFI. Specifically, during the course of the CosmoGlobe DR2 work, a new four-component MBB model, based on five astrophysical tracers, has emerged as a particularly compact and efficient description. Although a four-component model may at first sight appear as significantly more complicated than either the standard single-component MBB model adopted by the *Planck* team, or by the two-component MBB model pioneered by Finkbeiner et al. (1999), the key point in our new analysis is that all four components are well traced by well-known dust templates coupled with spatially isotropic SEDs. The number of degrees of freedom per pixel is therefore very small, allowing for a very rigid and compact statistical description.

Four of the five templates in this model are already known to be efficient dust tracers, namely 1) HI4PI H I line emission, tracing molecular gas; 2) *Gaia* extinction, tracing near-by dust absorption; 3) Dame et al. (2001b) CO line emission, tracing cold dust in star-forming regions; and 4) WHAM Hα line emission, tracing hot dust in ionized regions. However, in this paper and its companion papers, we additionally find that ionized carbon emission, as traced by the FIRAS C II 158 μm line emission map, is an excellent tracer of thermal dust emission with a temperature of $\sim$25-30 K. This observation may have far-reaching consequences for future studies and models of dust emission in the microwave and infrared regimes.

In the current paper, we perform a linear regression analysis of *Planck* HFI 353–857 GHz and DIRBE 3.5–100 μm data with this model, which demonstrates the validity of this key finding, even with a minimal set of assumptions. In a follow-up analysis by Sullivan et al. (2026), we perform a Bayesian analysis of *Planck* HFI data with the goal of deriving high-resolution templates of the H I and C II correlated components directly from microwave data. Finally, Gjerløw et al. (2026) applies this novel model to the *COBE*-DIRBE data.

The rest of the paper is organized as follows: in Sect. 2 we discuss the template fitting algorithm and in Sect. 3 the data used in the current paper; finally, in Sect. 4 we present the results from these calculations, before we conclude in Sect. 5.

2. Template fitting methodology

The main goal of this paper is to quantify the efficiency of known dust tracers for modelling thermal dust emission in the microwave and infrared frequency ranges. While all other papers in the current CosmoGlobe DR2 paper suite adopts a global Bayesian analysis framework as their computational engine (as

Table 1. Templates used for each frequency band.

Band	Freq. (GHz)	C ɪɪ	HI4PI	*Gaia*	WHAM	CO
Planck 353 GHz	353	✓	✓	✓	✓	✓
Planck 545 GHz	545	✓	✓	✓	✓	✓
Planck 857 GHz	857	✓	✓	✓	✓	✓
DIRBE 240 μm	1250	✓	✓	✓	✓	✓
DIRBE 140 μm	2100	✓	✓	✓	✓	✓
DIRBE 100 μm	3000	✓	✓	✓	✓	✓
DIRBE 60 μm	5000	✓	✓	✓	✓	
DIRBE 25 μm	12000	✓	✓			
DIRBE 12 μm	25000	✓				

implemented in the `Commander` code; Eriksen et al. 2004; Galloway et al. 2023), the analyses considered in this paper can be performed with much simpler template fitting tools. In addition to resulting in a much shorter computational run time, we also consider it valuable that the following results may be reproduced by other readers with a minimum of coding efforts and independently of `Commander`.

For each dataset[1] d_i at a given frequency band i, our basic data model reads

$$d_i = \sum_c a_{i,c} t_c + m_i + n_i, \qquad (1)$$

where the sum over c runs over $n_{\mathrm{comp}} = 5$ dust components, each with an amplitude $a_{i,c}$ and a spatial template t_c. In addition, we include a monopole term, m_i, and a white noise contribution, n_i. We assume that all data are provided as HEALPix[2] (Górski et al. 2005; Zonca et al. 2019) maps with identical angular and pixel resolution, and that the frequency maps only include dust emission and noise; other astrophysical components, such as CMB, CIB, or zodiacal light contributions are removed through preprocessing; see Sect. 3 for details.

Next, we define $a = \{a_c, m\}$ to be the vector of all free template and monopole amplitudes, for a total of six parameters per frequency channel, and we assume the noise to be Gaussian distributed with a covariance matrix N_i. Fitting a linear model to Gaussian data has a well-known solution, and reads

$$a_i = (T^T N^{-1} T)^{-1} T^T N^{-1} d, \qquad (2)$$

where we define T to be an $n_{\mathrm{pix}} \times (n_{\mathrm{comp}} + 1)$ template matrix such that matrix column c contains component template t_c and the final column contains the constant unity for the monopole. This equation is easily solved brute-force by matrix inversion.

The noise covariance, N, should ideally describe all sources of uncertainty, both systematic uncertainties and random noise. However, since we are working with a very low-dimensional data model fitted to datasets with extremely high signal-to-noise ratios, the random instrumental noise is negligible compared to calibration and modelling uncertainties, and we therefore set N equal to a constant in the following. Equation (2) therefore simplifies to

$$a_i = (T^T T)^{-1} T^T d, \qquad (3)$$

which is the standard normal equation for uniform weights.

---

[1] Bold symbols indicate a vector of n_{pix} HEALPix pixels.
[2] http://healpix.sourceforge.net/

Masking of bright or unobserved pixels is implemented simply by removing the relevant pixels in t and d. Specifically, we remove pixels very close to the Galactic plane, as well as any pixels excluded by the FIRAS processing mask. A total of 91 % of the sky is included the following analysis.

3. Data

3.1. Frequency maps

In this paper we consider only data for which thermal dust dominates strongly over other astrophysical contributions. Specifically, we consider the *Planck* High Frequency Instrument (HFI) 353, 545, and 857 GHz frequency maps (Planck Collaboration III 2020) and the six longest wavelength DIRBE bands from 240 μm to 12 μm.

For HFI, we use *Planck* PR4 (Planck Collaboration LVII 2020) frequency sky maps. From these, we subtract 1) the best-fit CMB dipole listed in the PR4 paper; 2) CMB fluctuations as estimated by the SMICA algorithm (Planck Collaboration IV 2018); 3) CIB fluctuations as estimated by the GNILC algorithm (Planck Collaboration Int. XLVIII 2016); and 4) an estimate of the stationary zodiacal light emission (Planck Collaboration XIV 2014). We have purposefully chosen to use products not generated by `Commander`, in order for this paper to be as independent of the main CosmoGLOBE DR2 analysis as possible.

Ideally, we would have preferred to use products that are independent of CosmoGLOBE DR2 also for DIRBE, but in this case the official products are too contaminated by zodiacal light residuals for our purposes. We therefore use the DIRBE frequency maps presented by Watts et al. (2024a). For these, no additional contributions are subtracted.

Since this work is primarily concerned with dust modeling, we attempt to avoid contamination from (especially) the CMB signal, which dominates at the lower *Planck* frequencies. To that end, we use only the HFI data from 353 to 857 GHz. All of the input frequency maps are taken from the *Planck* PR4 data release (Planck Collaboration LVII 2020).

The template fitting procedure described in Sect. 2 requires all maps to be smoothed to a common resolution – if not, the extra degrees of freedom at smaller scales in some of the maps and templates might bias the fit at larger scales. Out of all the data and templates used in this analysis, the *COBE*-FIRAS C ɪɪ map has the lowest native resolution. We therefore convolve all involved maps (except C ɪɪ) with the *COBE*-FIRAS beam, shown in Fig. 1 (taking into account the drift along Ecliptic meridians; e.g., Odegard et al. 2019), and repixelating to a common HEALPix resolution of N_{side}=16.

3.2. Thermal dust templates

To model the thermal dust contribution in HFI and DIRBE, we consider the five following dust tracers, plotted at full angular resolution in Fig. 2.

Ionized carbon — *COBE*-FIRAS C ɪɪ The *COBE*-FIRAS instrument (Mather et al. 1994) is the only currently available full-sky spectrometric survey in the microwave and infrared electromagnetic wavelengths. While the original science goal of the experiment was to measure the CMB monopole spectrum, it also provided a wealth of large-scale Galactic information as well. In particular, it provided the best full-sky measurement of Galactic 157.7 μm C ɪɪ emission published to date (Fixsen et al. 1998).
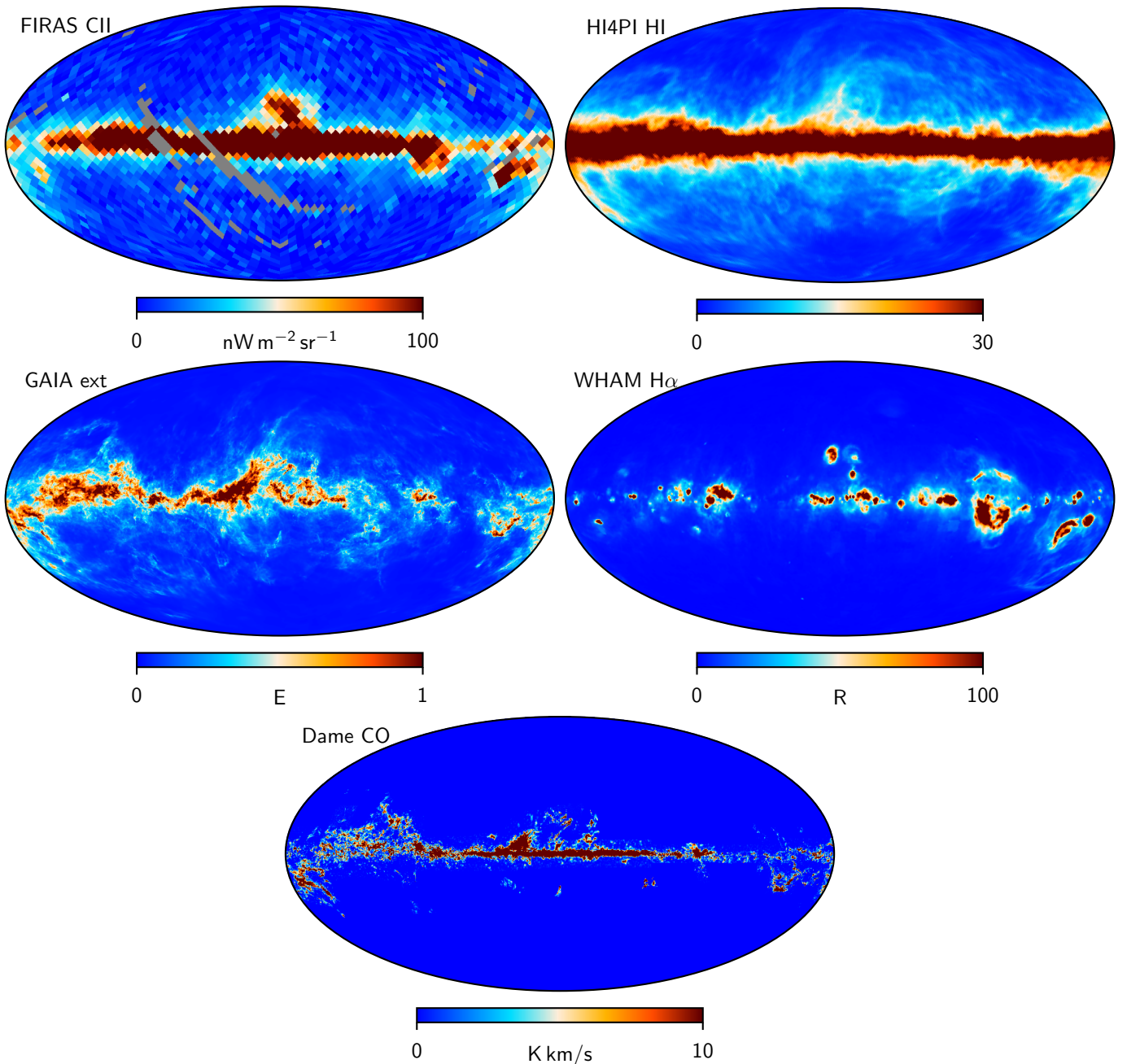
Fig. 2. Input maps of each of the following thermal dust tracers (from left to right and top to bottom): C ɪɪ 158 μm line emission from *COBE*-FIRAS, H ɪ line emission from HI4PI, dust extinction from *Gaia*, Hα line emission from WHAM, and CO line emission from Dame et al. (2001b). All maps are smoothed to the FIRAS beam and then used for the low-resolution template fitting at N_{side}=16.

C ɪɪ plays a key role in Galactic structure formation as a key cooling agent, and it has long been recognized as a powerful gas tracer; in the current paper, however, we consider its potential as a dust tracer.

Neutral hydrogen − HI4PI The HI4PI HI survey (HI4PI Collaboration: et al. 2016) is a full-sky survey of the 21 cm hydrogen line, performed by a combination of data from EBHIS and GASS. The 21 cm line has been used as a tracer for dust structures (Planck Collaboration XXIV 2011), and is typically associated with low-intensity regions of the sky, as it requires the hydrogen to not be ionized, but rather be in its lowest energy state.

Nearby dust through extinction − Gaia One source of important information about the 3-dimensional structure of dust is starlight extinction. By comparing expected stellar spectra with observed ones, Edenhofer et al. (2024) was able to reconstruct such dust structures up to a distance of 1.25 kpc, represented by a series of maps for each distance bin. Using the accompanying software, we integrated these maps out to their furthest distance, which still represents relatively close dust structures, and we use this as a template for nearby dust structures. The choice of the distance cut is driven by the available Edenhofer maps rather than any physical considerations.
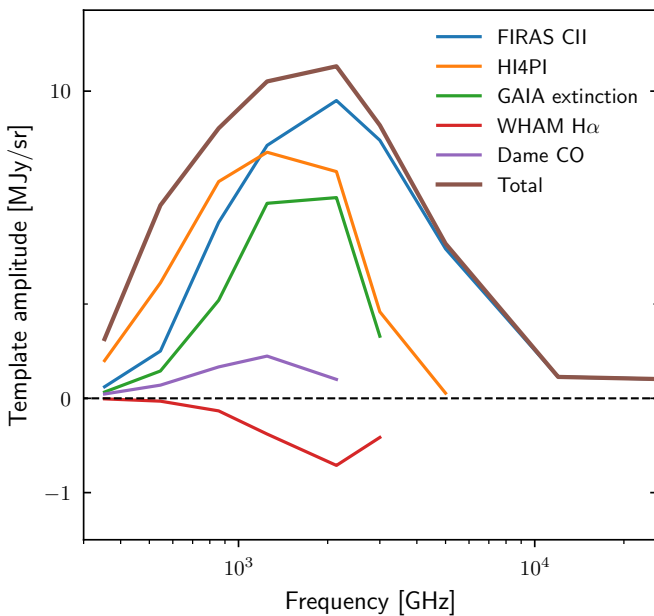
Fig. 3. Template amplitudes as a function of frequency for the nine channels used in this analysis, plotted only at the channels where they are fit. The WHAM Hα amplitudes are negative because it is an absorptive template.
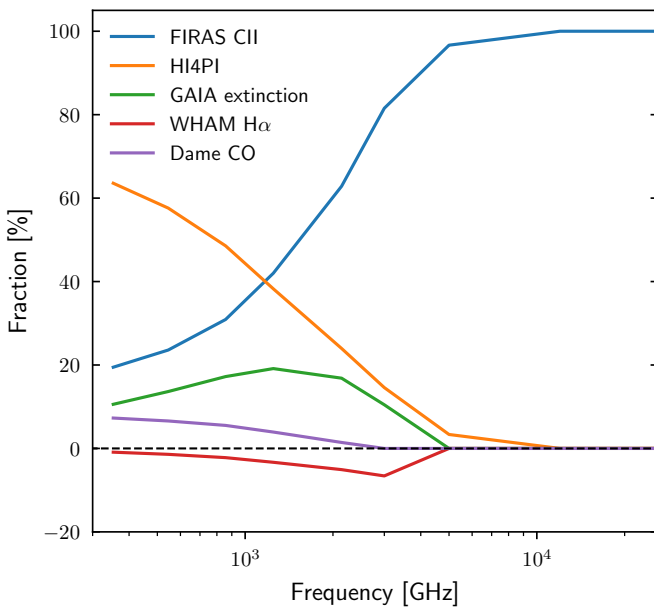

Fig. 4. Relative template amplitudes at each frequency in terms of the power contribution of each component as a percentage of the combined model amplitude.

Ionized hydrogen – WHAM   The Wisconsin Hα Mapper (WHAM) (Haffner et al. 2003b, 2010) surveyed the intensity of the Hα line over the whole sky, with a resolution of 1° FWHM and a velocity resolution of 12 km/s. This line is typically associated with higher energy regions, as it is most commonly emitted from hydrogen atoms recombining after ionization. The WHAM Hα map was used in early *Planck* analyses as a tracer of nearby free-free emission.

Carbon monoxide – Dame CO J = 1-0   Finally, Dame et al. (2001b) surveyed about 45% of the sky for the $J=1 \rightarrow 0$ CO line within 30 degrees of the Galactic equator. CO is a well-known tracer of cold dust surrounding star forming regions.

It is important to note that the relative importance of these tracers depend strongly on both frequency and position on the sky. When performing the first iteration of the analysis presented in the following, we made no assumptions regarding the relative contribution of each component, but simply fitted all five components freely to all channels. However, due to the fact that the set of five selected templates discussed here certainly represents an incomplete basis for the true dust signal, the fitted amplitudes for a given component tend to become unphysical when their signal-to-noise ratio approaches zero; rather than fitting an actual component, the fitting algorithm uses it to suppress modelling errors in the others, and the result is typically obvious "over-subtraction shadows" in the data-minus-model residual maps. For this reason, we exclude individual templates from the fit at the higher frequencies, once we observe through inspection of the resulting spectra and residuals that the component in question does not significantly improve the overall fit. Table 1 provides an overview of which templates are fitted to which frequency maps.

4. Results

4.1. Template amplitude fits

The template amplitudes per frequency band resulting from applying the algorithm in Sect. 2 are shown in Fig. 3. The thick brown curves shows the sum of all components. First, we note that all spectra show a characteristic bump with a peak frequency between ~1200 and 2000 GHz, which corresponds to MBB temperatures between 10 and 30 K; see below for actual temperature estimations of these spectra.

Second, at frequencies below ~1200 GHz the overall fit is dominated by HI4PI, which traces neutral hydrogen. This agrees well with our prior expectations, given the wide usage of HI as a dust tracer in the microwave regime (e.g., Planck Collaboration XVIII 2011; Lenz et al. 2017; Hensley & Draine 2023).

However, it is perhaps more surprising to note that the total fit above 1200 GHz is dominated by the FIRAS C II map. Indeed, above 3000 GHz C II is effectively the only tracer with a statistically significant contribution. This simple yet far-reaching observation represents the main finding in this paper.

Another potentially surprising result is that the Hα component appears with negative amplitudes in Fig. 3. This indicates that regions dominated by Hα acts as a dust extinction source in the current model, rather than an emission source. We have spent significant time trying alternative models and data configurations, but have found that this observation is extremely robust against data selection; whenever the Hα map is excluded, a blue imprint with a Hα-like morphology appears in the residuals.

A complementary view of these spectra is provided in Fig. 4, which shows the relative fraction of each component relative to the sum as a function of frequency. More than 60 % of the model is described by the HI component at 353 GHz, while at 1000 GHz the HI and C II contributes about 40 % each, with the nearby *Gaia* dust map accounting for most the remaining 20 %. The Hα and CO tracers account for roughly comparable quantities, but with opposite signs. Once again, we see that above 3000 GHz the C II component fully dominates.
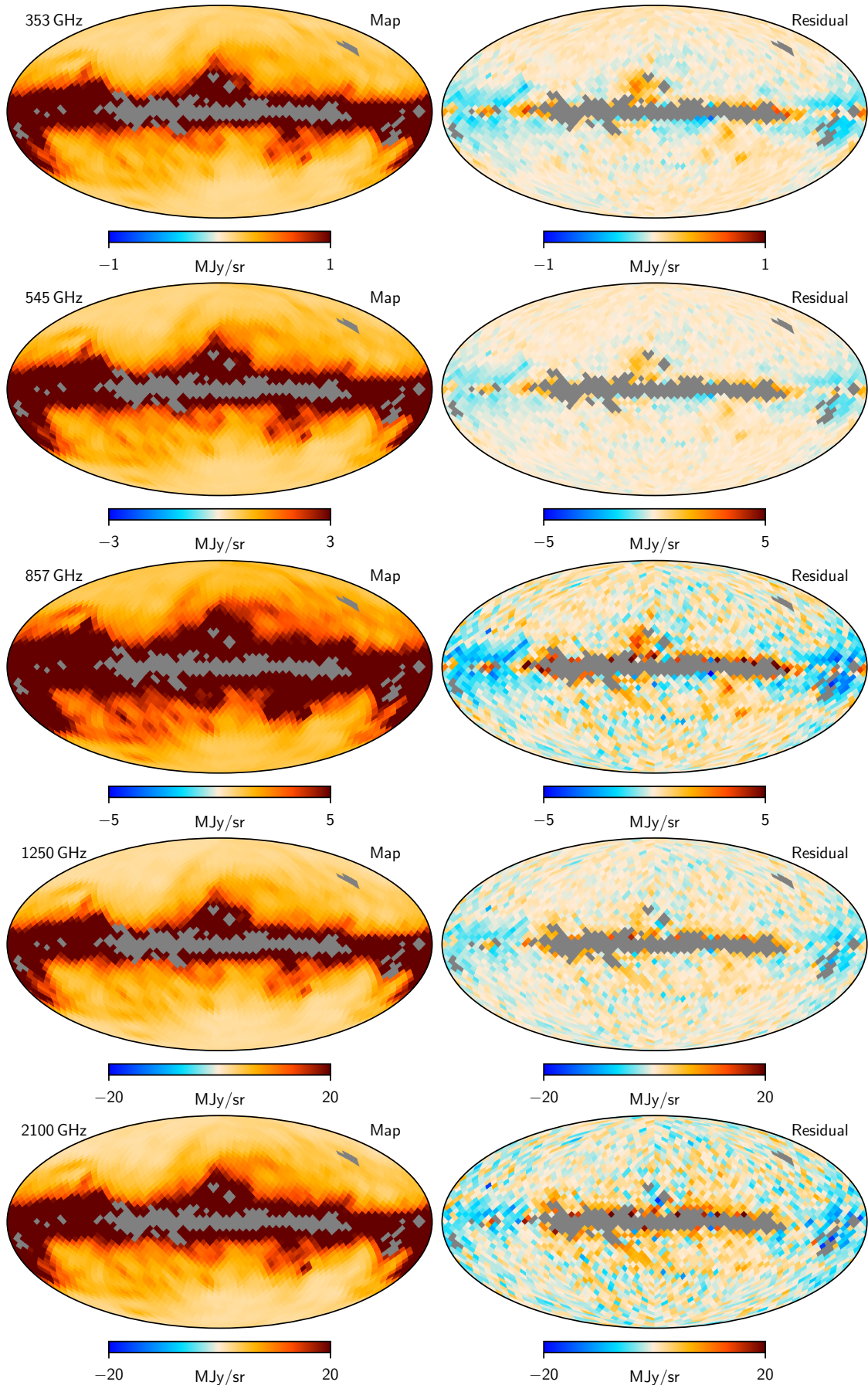
Fig. 5. Comparison between full (left column) and template cleaned (right) maps between 353 and 2100 GHz. The grey pixels are masked by the common analysis mask. All maps are convolved with the FIRAS beam.
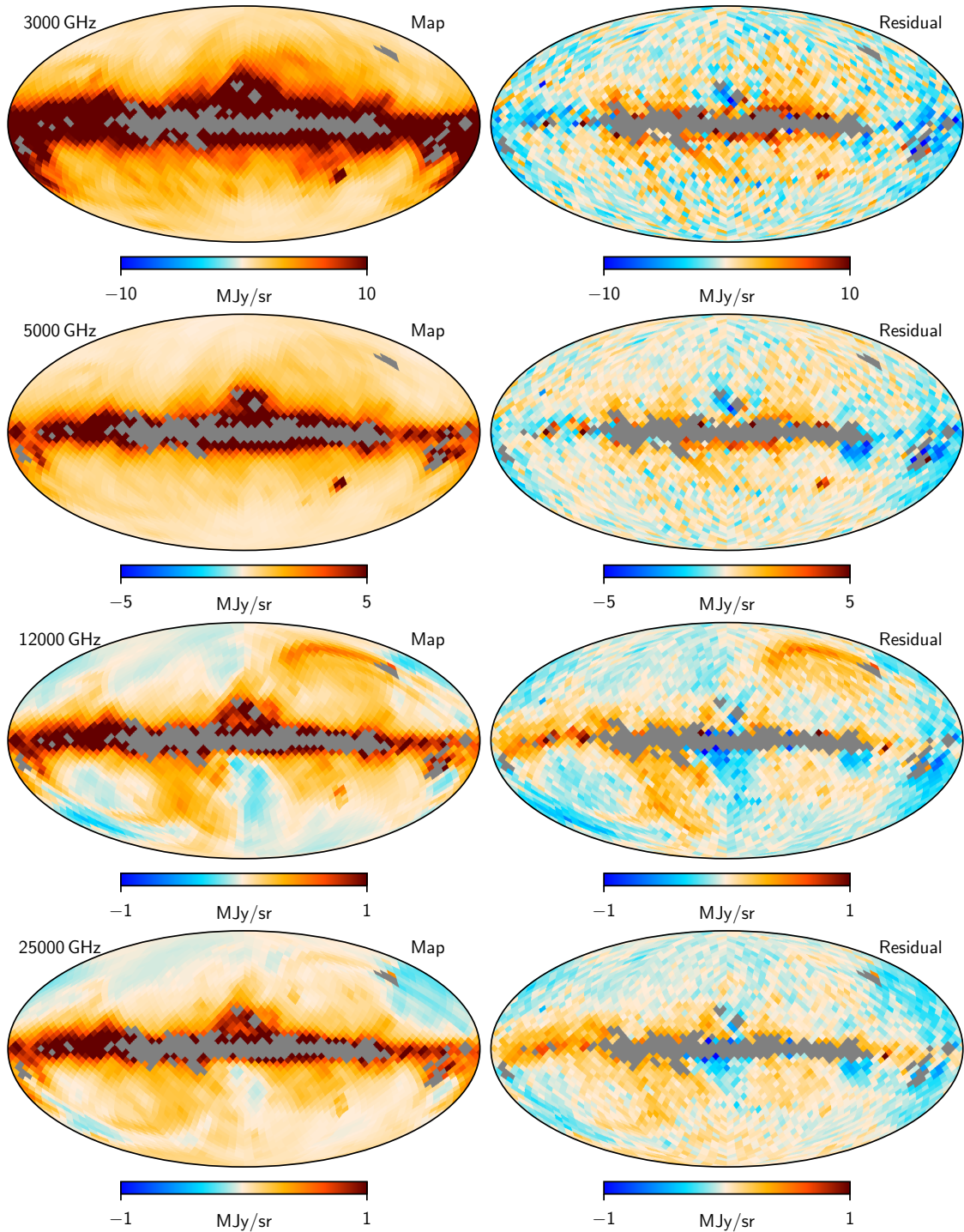
Fig. 6. Same as Fig. 5 but frequencies between 3000 and 25 000 GHz (100 μm - 12 μm).

4.2. Model efficiency and goodness-of-fit

In Figs. 5 and 6, we show a comparison between the original data (left columns) and the template cleaned maps (right columns). Clearly, the template fitting performs well for all frequencies, leaving residuals that are much smaller in amplitude than the original maps. The morphologies of those residuals appear to correlate with high-activity regions of the Milky Way, in particular at 857 GHz and 3000 GHz, as well as unmodelled zodiacal emission from the Solar System, which is most evident in the two highest frequency maps.

In order to quantify the degree to which these visual impressions bears out in practice, we show in Fig. 7 a measure of the amount of signal that is accounted for by the template fit. This measure is simply defined by the ratio between the variance difference between the raw data and the residual and the variance of the raw data itself. If the model happened to fully model the data, the residual variance would be zero, and the ratio would be unity; if the model happened to explain nothing of the data, the residual would be equal to the data, and the ratio would be zero. In Fig. 7 we see that this quantity ranges between 98 % at frequencies below 1000 GHz, and decreases to about 83 % at 12 000 GHz. In
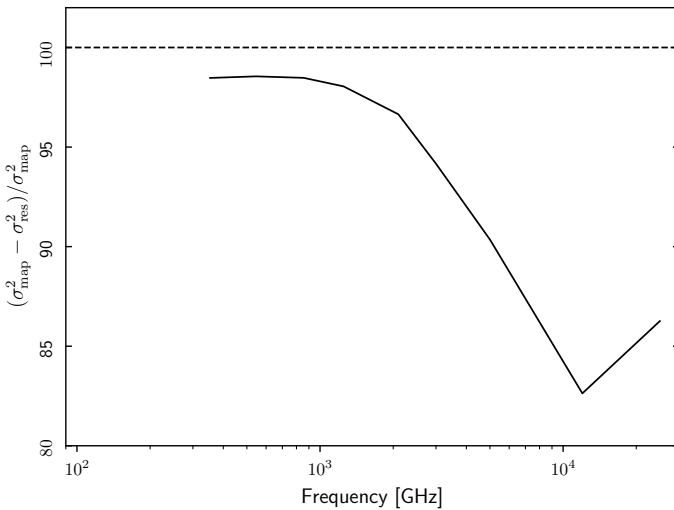
Fig. 7. Efficiency of the dust model at describing the data at at each frequency. We subtract the squared residuals from the squared map, and normalize by the amplitude of the map. The five component template-based dust model is able to recover more than 80% of the total map power at all frequencies, including those with known residual zodiacal contamination like 25 μm.

Fig. 8. Comparison between template fit amplitudes (solid lines, reproduced from Fig. 3) with best-fit modified blackbody models (dotted lines), in the thermal regime for each component. The best-fit MBB temperatures and spectral indices for each curve are listed in the figure legend.

this respect, it is important to note that zodiacal light residuals become gradually stronger with frequency, and they are particularly important at the DIRBE 25 and 12 μm channels.

It is also worth emphasizing that the only active dust tracer at 12 μm is C ɪɪ (see Table 1), and still the efficiency is higher than 85 %. This clearly demonstrates the power of the C ɪɪ map as a high-frequency dust tracer.

4.3. Modified blackbody fits

In Fig. 8, we fit a modified blackbody model to the template fitting SEDs,

$$s(\nu) = A \frac{\nu^{\beta+3}}{\exp\left(\frac{h\nu}{k_b T}\right) - 1}. \tag{4}$$

Here, A is an arbitrary scaling factor, T is the blackbody temperature, and β is the spectral index. It is especially interesting to compare the two strongest SEDs — those associated with the C ɪɪ and H ɪ templates, respectively — as we see that they correspond to significantly different temperatures. The H ɪ-correlated component has a best-fit temperature of about 16 K, while the C ɪɪ-correlated component has a best-fit temperature of about 25 K. The corresponding best-fit spectral indices are β = 1.40 and 1.56, respectively. For this reason, we refer to the H ɪ- and C ɪɪ-correlated components as "cold" and "hot dust" in our companion papers, although we note that the latter is often used about significantly higher temperatures in the literature.

The CO-correlated component corresponds to the lowest temperature, around 12 K. This component is known to trace cold and dense star-forming regions, and a lower temperature is therefore in good agreement with prior expectations.

Moving on to the nearby *Gaia* extinction template, we also find a somewhat low temperature, around 15 K, which is similar to the H ɪ temperature. However, we see that the actual SED peaks between the H ɪ and C ɪɪ SEDs, which is due to a very steep spectral index. In this respect, it is worth recalling that this nearby component has a lower amplitude, and therefore lower signal-to-noise ratio, than the two dominant components, and it
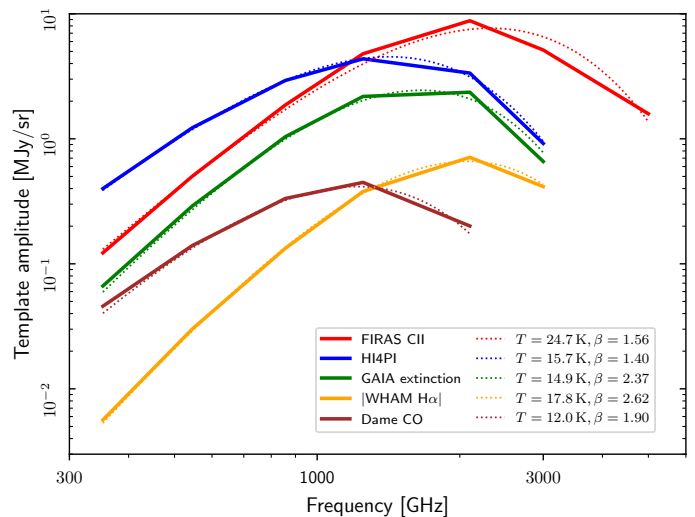
is therefore more susceptible to modelling errors and data selection effects. For comparison, when fitting these spectral parameters to HFI data, Sullivan et al. (2026) finds a best-fit MBB temperature for the nearby component of 18 K.

5. Conclusions

In this paper, we have fit five pre-existing dust tracers to ten *Planck* HFI and DIRBE frequency maps between 353 GHz and 25 THz. These include a FIRAS C ɪɪ template; an H ɪ HI4PI template; a "nearby dust" template constructed from integrated *Gaia* extinction maps; the Dame CO template; and a WHAM Hα template. We find that this simple template-based model is both able to account for more than 95% of the dust variance for all but the two highest frequency bands, and that the resulting SEDs follow physically reasonable modified blackbody curves up to about 3-5 THz.

The most important novel finding in this analysis is that the most efficient tracer of large-scale dust emission is C ɪɪ. The importance of C ɪɪ emission for Galactic structure, dynamics and cooling physics in general has been long recognized, but the fact that it also is an extremely efficient dust tracer is to our knowledge a new result. In fact, above 3000 GHz this component totally dominates the overall fit, and even at *Planck* HFI frequencies it is second only to H ɪ. The temperature of this C ɪɪ-correlated component is significantly higher than for either the H ɪ or nearby components, with a typical value of about 25 K.

This analysis indicates that it is possible to vastly reduce the complexity of the challenge of thermal dust modelling for both microwave and infrared regimes. Instead of operating with phenomenological models that involve multiple free parameters per pixel, a model based on multiple physical components, each with well-defined spectral parameters, could both lead to a lower number of degrees of freedom in total, and also provide a more direct way of imposing physically well-motivated priors and combining data sets. This general approach is applied in practice in two companion papers by Sullivan et al. (2026) and Gjerløw et al. (2026), who fit multi-component dust models to the full-resolution *Planck* HFI and DIRBE data, respectively.

A final key question arising from this analysis is whether these findings also apply to polarized dust emission, and this question will be the subject of a future analysis. If this turns out to be the case, it would have a significant impact on the feasibility of modelling polarized dust emission for future CMB experiments, which are dependent on accurate modelling of polarized foregrounds to reach the sensitivities required for their science goals (in particular, the detection of tensor-to-scalar ratio r). In particular, a key goal of future CMB B-mode experiments would then be to internally distinguish between hot and cold dust, which in turn would impose requirements on the frequency coverage of the experiment in question, with an increased focus on frequencies between 500 and 1000 GHz.

References

Ade, P., Aguirre, J., Ahmed, Z., et al. 2019, J. Cosmology Astropart. Phys., 2019, 056

BICEP2 Collaboration. 2018, Phys. Rev. Lett., 121, 221301

Dame, T. M., Hartmann, D., & Thaddeus, P. 2001a, ApJ, 547, 792

Dame, T. M., Hartmann, D., & Thaddeus, P. 2001b, ApJ, 547, 792

Draine, B. T. 2011, Physics of the Interstellar and Intergalactic Medium (Princeton University Press)

Edenhofer, G., Zucker, C., Frank, P., et al. 2024, A&A, 685, A82

Eriksen, H. K., O'Dwyer, I. J., Jewell, J. B., et al. 2004, ApJS, 155, 227

Finkbeiner, D. P., Davis, M., & Schlegel, D. J. 1999, ApJ, 524, 867

Fixsen, D. J., Bennett, C. L., & Mather, J. C. 1998, arXiv e-prints, astro

Galloway, M., Andersen, K. J., Aurlien, R., et al. 2023, A&A, 675, A3

Gjerløw et al. 2026, A&A, in preparation [arXiv:20xx.xxxxx]

Górski, K. M., Hivon, E., Banday, A. J., et al. 2005, ApJ, 622, 759

Haffner, L. M., Reynolds, R. J., Babler, B. L., et al. 2016, in American Astronomical Society Meeting Abstracts, Vol. 227, American Astronomical Society Meeting Abstracts #227, 347.17

Haffner, L. M., Reynolds, R. J., Madsen, G. J., et al. 2010, in American Astronomical Society Meeting Abstracts, Vol. 215, American Astronomical Society Meeting Abstracts #215, 415.28

Haffner, L. M., Reynolds, R. J., Tufte, S. L., et al. 2003a, ApJS, 149, 405

Haffner, L. M., Reynolds, R. J., Tufte, S. L., et al. 2003b, ApJS, 149, 405

Hauser, M. G., Arendt, R. G., Kelsall, T., et al. 1998, ApJ, 508, 25

Hensley, B. S. & Draine, B. T. 2023, ApJ, 948, 55

HI4PI Collaboration:, Ben Bekhti, N., Flöer, L., et al. 2016, A&A, 594, A116

Kelsall, T., Weiland, J. L., Franz, B. A., et al. 1998, ApJ, 508, 44

Kondo, T., Ishihara, D., Kaneda, H., et al. 2016, AJ, 151, 71

Lenz, D., Hensley, B. S., & Doré, O. 2017, ApJ, 846, 38

LiteBIRD Collaboration, Allys, E., Arnold, K., et al. 2023, Progress of Theoretical and Experimental Physics, 2023, 042F01

Mather, J. C., Cheng, E. S., Cottingham, D. A., et al. 1994, ApJ, 420, 439

Miville-Deschênes, M.-A. & Lagache, G. 2005, ApJS, 157, 302

O'Brien, R., Arendt, R. G., Windhorst, R. A., et al. 2025, arXiv e-prints, arXiv:2510.18231

Odegard, N., Weiland, J. L., Fixsen, D. J., et al. 2019, ApJ, 877, 40

Pan-Experiment Galactic Science Group. 2025, The Astrophysical Journal, 991, 23

Paradis, D., Dobashi, K., Shimoikura, T., et al. 2012, A&A, 543, A103

Planck Collaboration XVIII. 2011, A&A, 536, A18

Planck Collaboration XXIV. 2011, A&A, 536, A24

Planck Collaboration XI. 2014, A&A, 571, A11

Planck Collaboration XIV. 2014, A&A, 571, A14

Planck Collaboration X. 2016, A&A, 594, A10

Planck Collaboration III. 2020, A&A, 641, A3

Planck Collaboration IV. 2018, A&A, 641, A4

Planck Collaboration Int. XLVIII. 2016, A&A, 596, A109

Planck Collaboration LVII. 2020, A&A, 643, A42

Reach, W. T., Dwek, E., Fixsen, D. J., et al. 1995, ApJ, 451, 188

San, M. et al. 2024, A&A, in preparation [arXiv:20xx.xxxxx]

Sano, K., Kawara, K., Matsuura, S., et al. 2016, ApJ, 818, 72

Schlegel, D. J., Finkbeiner, D. P., & Davis, M. 1998, ApJ, 500, 525

Sullivan et al. 2026, A&A, in preparation [arXiv:20xx.xxxxx]

Watts, D., Galloway, M., Gjerlow, E., et al. 2024a, A&A, submitted [arXiv:2408.10952]

Watts, D. et al. 2024b, A&A, in preparation [arXiv:2406.01491]

Zonca, A., Singer, L., Lenz, D., et al. 2019, Journal of Open Source Software, 4, 1298